GPS Solut (2017) 21:1013–1025
DOI 10.1007/s10291-016-0589-y

ORIGINAL ARTICLE

Brazilian active GNSS networks as systems for monitoring the ionosphere

Vinícius Amadeu Stuani Pereira[1] · **Paulo de Oliveira Camargo**[1]

Received: 1 March 2016 / Accepted: 24 November 2016 / Published online: 5 December 2016

Abstract This research shows the viability of using Global Navigation Satellite System (GNSS) stations from Brazilian active networks in monitoring the ionosphere. Various indexes of ionospheric irregularities and scintillation of GNSS signals, estimated in real-time and post-processed from GNSS data, are explored for this purpose. This way, an increase in the spatial resolution of ionospheric information is provided, allowing the generation of maps of scintillation and irregularities in observing the spatial and temporal behavior of the layer's activity cycle, since the number of ionosondes, imagers, and radars is insufficient for monitoring the irregularities in Brazil. Experiments to evaluate the estimates of the indexes are performed for periods of high and low variability of electrons. Three Brazilian networks are used: the Brazilian Network for Continuous Monitoring (RBMC), the GNSS Active Network of Sao Paulo State (GNSS-SP), and CIGALA/CALIBRA. The results are compared with data from ionosondes and PolaRxS-PRO Septentrio receivers, proving compatible with moderate to high correlations. An analysis of the seasonal variation during the peak of solar cycle 24 is carried out. The maps allow identifying the displacement of ionospheric irregularities along the magnetic equator over Brazil, from northeast to southwest, starting at 7:00 pm and ending at 2:00 am local time. Real-time monitoring is carried out for the summer solstice in the southern hemisphere, and results are consistent with those from the post-processed mode. The indexes and maps can be applied to the analysis of GNSS positioning. Real-time ionospheric information can be used in important practical applications because the displacement monitoring of irregularities allows prior knowledge of whether there will be a deterioration of positioning accuracy in a certain region.

Keywords Ionospheric irregularities · Ionospheric scintillation · Index f_P · Index F_P · Index *ROTI* · Index σ_Φ

Introduction

One of the factors limiting Global Navigation Satellite System (GNSS) positioning is the ionosphere. The variation in electron density causes an effect called ionospheric scintillation. Ionospheric scintillations can generate variations of amplitude, phase, angle, and polarization of the GNSS signal when it passes through a region of irregularities in the electron density (Klobuchar 1996).

The scintillations are strong in auroral zones and tropical regions during the night near the spring and autumn equinoxes. The occurrence of scintillation increases during periods of high solar activity and other extreme activities such as the occurrence of geomagnetic storms (Conker et al. 2003; Davies 1990). In Brazil, the scintillation events are minimal from May to August and are at their greatest from September to April.

Using experiments already performed by Pereira and Camargo (2013), Oladipo and Schüler (2013), Chu et al. (2008), and Shan et al. (2002), it is possible to conduct studies of the behavior of the ionospheric layer from GNSS data of the Active Control Systems (ACS). Based on these data, the Total Electron Content (TEC), the Rate of Change

✉ Vinícius Amadeu Stuani Pereira
vi_stuani@hotmail.com

Paulo de Oliveira Camargo
paulo@fct.unesp.br

[1] Sao Paulo State University – UNESP, Roberto Simonsen, 305, Presidente Prudente, SP 19060-900, Brazil

of TEC (ROT), ionospheric irregularity indexes, and ionospheric scintillation indexes can be calculated. Maps of scintillation and irregularities can also be generated, which allow observation of spatial and temporal behavior and an understanding of the layer's activity cycle.

Because of the peak of solar cycle 24 in 2013–2014–2015, studies of the effects of the ionosphere on the propagation of GNSS signals have been conducted in Brazil in two projects: Concept for Ionospheric Scintillation Mitigation for Professional GNSS in Latin America (CIGALA) and Countering GNSS High Accuracy Applications Limitations due to Ionospheric Disturbances in Brazil (CALIBRA), both under the auspices of the European Union. During the projects, twelve PolaRxS-PRO Septentrio receivers were deployed, composing the CIGALA/CALIBRA network. Information about the data availability is accessible on: http://is-cigala-calibra.fct.unesp.br/is/stations/fixed.php?lan=en.

Another important active network is the Brazilian Network for Continuous Monitoring (RBMC), established by the Brazilian Institute of Geography and Statistics (IBGE). It is currently composed of more than 130 stations, of which 98 transmit data in real-time, forming the RBMC—Internet Protocol (RBMC-IP). The 20 stations of the GNSS Active Network of Sao Paulo State (GNSS-SP) also transmit data in real-time.

Figure 1 shows the Brazilian active networks. Information of each station, such as receiver, antenna, and coordinates, can be obtained in the files available on ftp://geoftp.ibge.gov.br/informacoes_sobre_posicionamento_geodesico/rbmc/relatorio/, and the data accessed on http://www.ibge.gov.br/home/geociencias/download/tela_inicial.php?tipo=8.

Due to the lack of dedicated instruments to monitor the ionospheric layer in Brazil, the objective has been to use

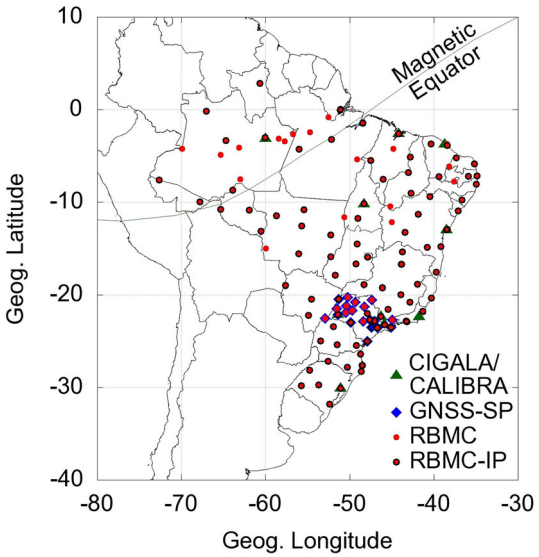

Fig. 1 Map of active GNSS networks in Brazil (as of 2016)

Brazilian ACSs as a system for monitoring the ionospheric irregularities and scintillations of GNSS signals, either in the post-processed mode or mainly in real-time. Applications such as precision agriculture, the approach and landing of aircraft, monitoring of oil rigs and structures, geodetic positioning, and Real-Time Kinematic (RTK) would be benefited with the real-time monitoring. In this way, the stations receiving GNSS signals are "transformed" into stations monitoring ionospheric activities.

Indexes of ionospheric irregularities and scintillation of GNSS signals

Several indexes can be used to assess ionospheric activities. They can be obtained from (a) ionosondes data such as *AI index* (Bremer et al. 2006), or *AI modified index* (Mielich and Bremer 2010); (b) IONEX files: W_p and *W-index* (Gulyaeva and Stanislawska 2008 and Gulyaeva et al. 2013); and (c) GNSS measurements: I_{ROT} (Wanninger 1993), *ROTI* (Pi et al. 1997), f_P and F_P (Mendillo et al. 2000), and *DIX* (Jakowski et al. 2012). The scintillations that GNSS signals suffer due to irregularities in the ionosphere can be quantified by the indexes σ_Φ (Van Dierendonck et al. 1993), *S4* (Conker et al. 2003), S_Φ (Forte 2005), and σ_{CHAIN} (Mushini et al. 2012). There are also solar and geomagnetic indexes that provide the level of ionospheric ionization and the strength of ionospheric distortions in the vertical and horizontal plasma distribution, such as Zurich sunspot number, solar radio flux at 10.7 cm (Jakowski et al. 1999), and geomagnetic K_p, A_p, and D_{st} (Campbell 1996). These are presented in the following the indexes of ionospheric irregularities f_P, F_P, I_{ROT}, and *ROTI*, and the indexes of ionospheric scintillation σ_Φ, S_Φ, and σ_{CHAIN}.

Estimates of irregularity indexes are based on ROT, which is calculated through the ratio of the difference of the TEC obtained consecutively between two epochs, and the time interval elapsed between the respective determinations:

$$\mathrm{ROT} = \frac{\mathrm{TEC}_{t_2} - \mathrm{TEC}_{t_1}}{t_2 - t_1} = \frac{\Delta \mathrm{TEC}}{\Delta t} \tag{1}$$

TEC can be obtained from the linear geometry-free combination, involving the phase measurements Φ^s_{1r} and Φ^s_{2r} of the L1 and L2 carriers (Matsuoka and Camargo 2004):

$$\mathrm{TEC}^s_r = \frac{f_1^2 f_2^2}{40.3\left(f_1^2 - f_2^2\right)}\left[\left(\lambda_2 \Phi^s_{2r} - \lambda_1 \Phi^s_{1r}\right) - \left(\lambda_1 N^s_{1r} - \lambda_2 N^s_{2r}\right) - e_{\Phi_{12}}\right] \tag{2}$$

where f_1, f_2, λ_1, λ_2, N^s_{1r}, and N^s_{2r} are the frequencies, wavelengths, and ambiguities of the carriers L1 and L2, respectively, and $e_{\Phi_{12}}$ contains the systematic errors not eliminated in the linear combination and random errors.

Substituting (2) into (1) gives an estimate of the ROT having only phase measurements of the L1 and L2 carriers at the t_1 and t_2 epochs as parameters:

$$\mathrm{ROT} = \frac{9.52 \times 10^{16}\left[\lambda_2\left(\Phi^s_{2rt_2} - \Phi^s_{2rt_1}\right) - \lambda_1\left(\Phi^s_{1rt_2} - \Phi^s_{1rt_1}\right)\right]}{t_2 - t_1} \tag{3}$$

where the ROT from (3) is used for GPS satellites, which are based on Code Division Multiple Access (CDMA). However, for GLONASS, which uses multiple divisions of frequencies to distinguish each satellite (FDMA), one should use:

$$\mathrm{ROT} = \frac{\frac{f_1^2 f_2^2}{40.3\left(f_1^2 - f_2^2\right)}\left[\lambda_2\left(\Phi^s_{2rt_2} - \Phi^s_{2rt_1}\right) - \lambda_1\left(\Phi^s_{1rt_2} - \Phi^s_{1rt_1}\right)\right]}{t_2 - t_1} \tag{4}$$

where f_1, f_2, λ_1, and λ_2 are the frequencies and wavelengths of the carriers L1 and L2 of each satellite observed.

The f_P irregularity index is the median value of the absolute of ROT for a period of 15 min, and ROT is being estimated every minute. The index is calculated for each satellite at a particular station, in order to represent the spatial resolution of ionospheric irregularities (Mendillo et al. 2000):

$$f_\mathrm{P}(n, hr, i) = \mathrm{Median}|\mathrm{ROT}| \tag{5}$$

where n is the satellite number, hr is the full hour (0–24 UT), and i is the 15-min time section within an hour ($i = 1, \ldots, 4$).

The F_P index is estimated for each station at each full hour. It represents the average value of the f_P indexes obtained for all satellites observed at a station in 1 h (Mendillo et al. 2000):

$$F_\mathrm{P}(\mathrm{hr}) = \frac{\sum_n^{\mathrm{nsat}}\left[\sum_i^k f_P(n, \mathrm{hr}, i)/k\right]}{\mathrm{nsat(hr)}} \times 1000 \tag{6}$$

where *nsat* corresponds to the total number of satellites observed during the period of an hour and k is the number of f_P values available in each hour ($k = 0, \ldots, 4$).

The index is intended to depict the general level of ionospheric irregularities present in the vicinity of a station. A value of $F_\mathrm{P} \leq 50$ represents low levels of irregularities, $50 < F_\mathrm{P} \leq 200$ indicates the presence of moderate irregularities, and $F_\mathrm{P} > 200$ represents the occurrence of strong levels of ionospheric irregularity (Mendillo et al. 2000).

Wanninger (1993) is apparently the first researcher to suggest that 30 s RINEX data could be used to characterize phase fluctuations as a diagnostic of ionospheric irregularities. He introduces the I_ROT index in order to simplify phase fluctuation detection. The index is computed over a 15-min period by:

$$I_\mathrm{ROT} = 10 \times \mathrm{RMS(ROT)} \tag{7}$$

where RMS is the Root-Mean Square of the ROT.

Wanninger (1993) does not present a classification standard for the I_ROT index. He concludes only that values close to or greater than 3 characterize strong ionospheric irregularity. Thus, Pereira and Camargo (2014) conducted an experiment to determine a classification standard for I_ROT, obtaining the following thresholds: $I_\mathrm{ROT} \leq 0.5$ for low level irregularities, $0.5 < I_\mathrm{ROT} \leq 2.0$ for moderate irregularities, and $I_\mathrm{ROT} > 2.0$ for strong levels of irregularities.

Pi et al. (1997), concerned that smaller-scale fluctuations were not being identified, suggest that an index for the rate of change of TEC can be determined based on the standard deviation of the ROT in a 5-min interval. Called *ROTI*, the index is obtained from the following equation:

$$\mathrm{ROTI} = \sqrt{\langle \mathrm{ROT}^2 \rangle - \langle \mathrm{ROT} \rangle^2} \tag{8}$$

where $< >$ represents the average.

A classification standard for the *ROTI* index was also determined: $ROTI \leq 0.05$ represents low levels of irregularities, $0.05 < ROTI \leq 0.2$ indicates moderate irregularities, and when $ROTI > 0.2$ the occurrence of strong levels of ionospheric irregularities is represented (Pereira and Camargo 2014).

The propagation of GNSS signals through regions of ionospheric irregularity can cause rapid variations in signal phase, known as phase scintillations. Strong phase scintillations can lead to cycle slips and loss of synchronization between the receiver and satellite. These scintillations are quantified by the σ_Φ index:

$$\sigma_\Phi = \sqrt{\langle \Phi_\mathrm{e}^2 \rangle - \langle \Phi_\mathrm{e} \rangle^2} \tag{9}$$

which consists of the standard deviation of detrended phase observations Φ_e. The Φ_e are collected at a high frequency of 50 Hz at an interval of 60 s and is commonly known as Φ_{60} (Van Dierendonck et al. 1993).

The σ_Φ index is given in radians and can also be expressed in degrees and meters. Hegarty et al. (2001) present the following classification standard for L1: very weak scintillation: $0.05 \text{ rad} < \sigma_\Phi \leq 0.2$ rad, weak scintillation: $0.2 \text{ rad} < \sigma_\Phi \leq 0.3$ rad, moderate scintillation: $0.3 \text{ rad} < \sigma_\Phi \leq 0.6$ rad, and strong scintillation: $\sigma_\Phi > 0.6$ rad.

The S_Φ phase scintillation index is suggested by Forte (2005) as an alternative to the σ_Φ index. Given in rad/s, it is calculated by the expression:

$$S_\Phi = \sqrt{\left\langle \left(\frac{\partial \Phi_\mathrm{e}}{\partial t}\right)^2 \right\rangle} \tag{10}$$

where S_Φ takes into account the rate of change of phase fluctuations of the carrier, being more consistent when using different methods of detrending, according to Forte (2005).

The CHAIN phase scintillation index, introduced by Mushini et al. (2012) and represented by σ_{CHAIN}, is the result of a change in the S_Φ index:

$$\sigma_{\mathrm{CHAIN}} = \sqrt{\left\langle \left(\frac{\partial \Phi_{\mathrm{e}}}{\partial t} \right)^2 |\Phi_{\mathrm{e}}| \right\rangle} \quad (11)$$

σ_{CHAIN} uses amplitude fluctuations as well as the rate of change of phase fluctuations.

Brazilian active GNSS networks as systems for monitoring the ionosphere

An algorithm is developed to estimate indexes of irregularities and phase scintillations, called Ion_Index (Pereira and Camargo 2016). The indexes are calculated from phase measurements of the carriers L1 and L2, recorded by GNSS receivers from Brazilian active networks. The flowchart of the algorithm is shown in Fig. 2, which is divided into two modes: post-processed (Ion_Index_PP) and real-time (Ion_Index_RT).

Except for the *S4* index, the ionospheric scintillation indexes are obtained by using detrended phase observations Φ_{e}. Several detrending methods can be found in the literature such as the Butterworth filter, polynomial fitting, and filtering by Continuous Wavelet Transform. However, most of these methods were developed taking into account phase measurements sampled at high frequencies in the order of 50 Hz, which apply a cutoff frequency of 0.1 Hz to separate the scintillation components from other components. In the case of phase measurements from the Brazilian ACSs, the sampling frequency is only 0.067 Hz, i.e., an observation every 15 s, which prevents the application of any of these detrending methods. Therefore, obtaining Φ_{e} values is restricted to removing multipath effects based on the application of an elevation mask, as well as detecting and not considering observations in which cycles loss occurs (Blewitt 1990). This approach provides plausible Φ_{e} values, allowing the estimates of phase scintillation indexes.

Different from the post-processed mode, where all stations of the three active networks can be selected for processing

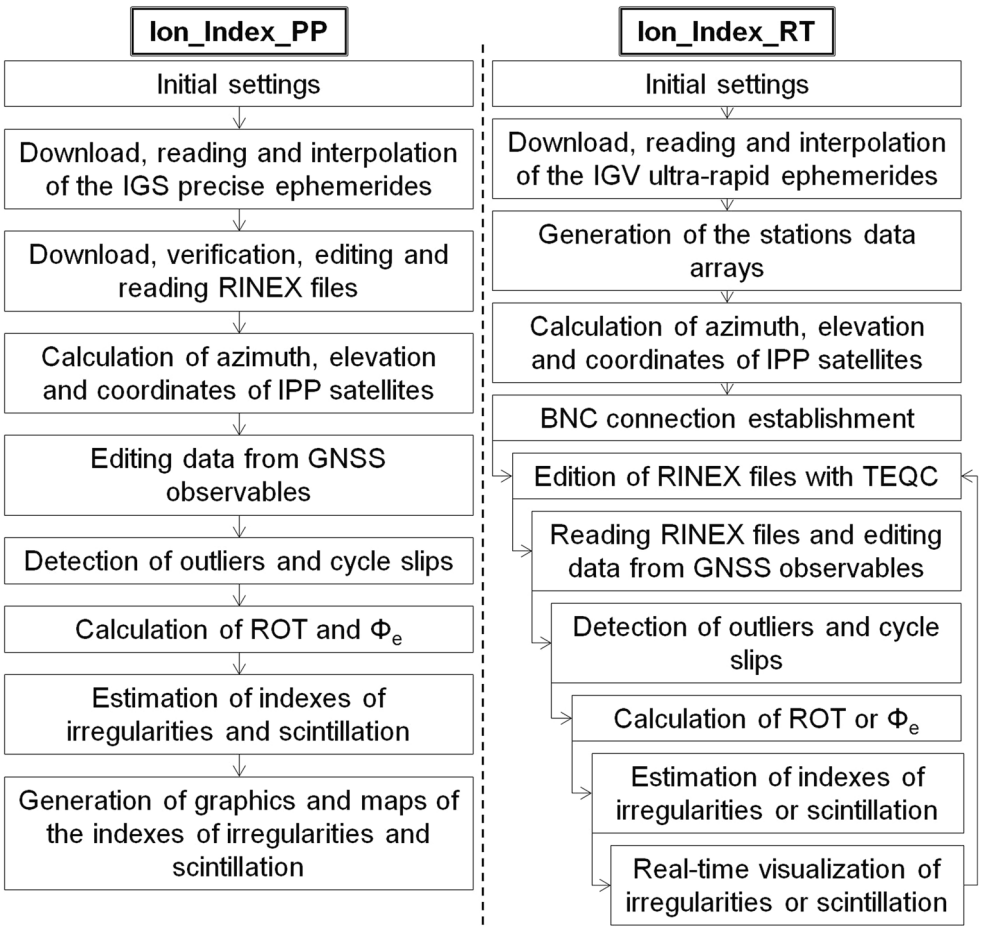

Fig. 2 Flowchart of Ion_Index. The algorithm estimates indexes of ionospheric irregularities and phase scintillations in two modes: post-processed (Ion_Index_PP) and real-time (Ion_Index_RT). IPP (Ionospheric Pierce Point) is the point where the satellite signal intercepts the ionospheric layer at a given mean height, and the IGV ultra-rapid ephemerides contain the Cartesian coordinates of the GPS and GLONASS satellites, and Φ_{e} means detrended phase observations. The editing GNSS observations consist of checking each epoch if observations in L1 and L2 are available, and detection of outliers and cycle slips using the commonly used Blewitt algorithm

totaling 143 stations, only 98 stations from RBMC-IP and 20 stations from GNSS-SP are available in real-time mode.

The real-time processing starts with the BKG NTRIP Client (BNC) connection. The ionospheric irregularity index of interest is estimated based on the ROT values, or, if one of the scintillation indexes has been selected, detrended phase measurements are used. However, to estimate the selected index per second, the concept of a moving window is applied, where the window is equal to the period of data of the selected index and the displacement is one second (Pereira and Camargo 2016).

Assessment the estimation of indexes

Irregularity indexes are estimated for the stations BOAV (2.8°N, 60.7°W) and CEFT (3.7°S, 38.5°W) for February 28 and March 1, 2014 (Days A and B, respectively). These days are characterized by strong levels of irregularities due to increased variability of electrons near the autumnal equinox and a negative incursion of the D_{st} index, which fluctuated between 0 and −100 nT (moderate geomagnetic storm). Three F-region ionospheric parameters are taken from the Brazilian Institute for Space Research (INPE) ionosondes at Fortaleza (3.7°S, 38.6°W) and Boa Vista (2.8°N, 60.7°W) also for these 2 days: minimum virtual height of the F-region ($h'F$), height of the peak electron density of the F2-layer (*hmF2*), and the critical frequency of the F2-layer (*foF2*). Values of *foF2* are taken in order to calculate the maximum electron density of the F2-layer (*NmF2*). The ionospheric indexes and parameters are compared in order to assess the estimation of ionospheric irregularity indexes from the Ion_Index.

Figure 3 shows the ionospheric irregularity indexes of station BOAV and the ionospheric parameters of the ionosonde Boa Vista for Day A. Figure 4 shows the CEFT indexes and Fortaleza parameters also for Day A. An elevation mask of 35° is considered. In the panels (b) to (d), the green line indicates the threshold between low and moderate levels of irregularities, while the red line indicates the boundary between moderate and strong levels.

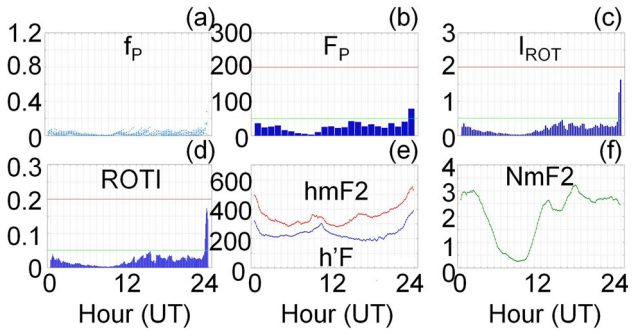

Fig. 3 Irregularity indexes of station BOAV in the panels (**a**–**d**) and ionospheric parameters of ionosonde Boa Vista in the panels **e** and **f** on Feb. 28, 2014. In panel **e** the height unit is meters, *hmF2* (*red*) means height of the peak electron density of the F2-layer, and $h'F$ (*blue*) means minimum virtual height of the F-region. In panel **f**, the unit of maximum electron density of the F2-layer (*NmF2*) is $10^{12}\mathrm{el}/\mathrm{m}^3$. The distance between station and ionosonde is 5 km

Analyzing Fig. 3, panels (b–d), it is noted that the values remained below the low level thresholds of ionospheric irregularities for most of the day, except for 23–24 UT, where the value of F_P is higher than 50 and I_{ROT} and *ROTI* values are higher than 0.5 and 0.05, respectively, characterizing moderate irregularities. This indicates that the I_{ROT} and *ROTI* indexes detail the ionospheric irregularities better than the F_P index, due to the fact that both are obtained from periods of data lower than the F_P index. Thus, the I_{ROT} and *ROTI* identify fluctuations in the signal on a small scale, whereas the F_P depicts the overall level of irregularities.

Comparing the instants when the values of the indexes of irregularities rose in Fig. 3, panels (a–d), with the respective moments of the parameters $h'F$ and *hmF2* in panel (e), a temporal correlation is observed. In the hours 00–01 and 23–24 UT, the basis of the F ionospheric layer has strong increases of 321 and 390 km, respectively, enough to start the processes of generating ionospheric irregularities at a scale capable of generating fluctuations in the phase of GNSS signals. This is corroborated by the increase in the heights of the peak ionization, 495 and 542 km, respectively. For other hours, the *hmF2* and $h'F$ values remained relatively low, around 285 and 210 km, respectively. These irregularities have no amplitudes capable of causing fluctuations in the GNSS signals, which can be checked in the values of irregularity indexes.

For Day B, the irregularity indexes of the station BOAV present a similar behavior. The duration and level of ionospheric irregularities in the hours 00–04 UT are higher, reaching an F_P around 140, I_{ROT} above 2 and *ROTI*

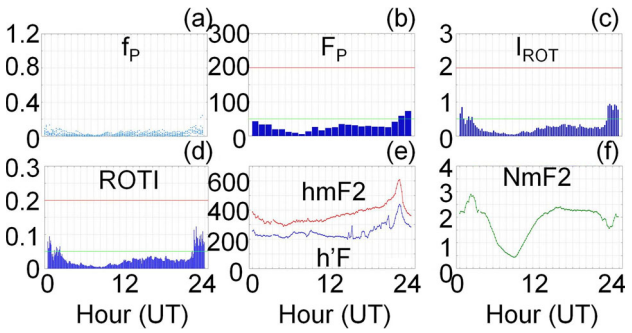

Fig. 4 Irregularity indexes of station CEFT in panels (**a**–**d**) and ionospheric parameters of ionosonde Fortaleza in panels **e** and **f** on Feb. 28, 2014. In panel **e**, the height unit is meters and in panel **f** the unit of *NmF2* is $10^{12}\mathrm{el}/\mathrm{m}^3$. The distance between station and ionosonde is 9 km

exceeding 0.2. It is noted that, considering the F_P index, the irregularities are classified as moderate. Already the values of I_{ROT} and *ROTI* indicate strong irregularities. This is justified by the periods of data and the way the indexes are calculated: The F_P is based on the f_P index, which in turn is obtained by the median of the ROT, and I_{ROT} is the RMS, and *ROTI* is the standard deviation of the ROT.

In relation to the Boa Vista ionosonde parameters for Day B, during the period 00–04 UT the values of $h'F$ and *hmF2* are higher when compared with the same period on Day A. The $h'F$ parameter presents an average value of 250 km, with a maximum of 352 km, and the ionization peak height has an average of 320 km, with a maximum of 435 km. The maximum electron density of the F2-layer corroborates the behavior of the irregularity indexes, because during 00–04 UT there is a rise in the electron density, obtaining a maximum of $2.8 \times 10^{12}\text{el}/\text{m}^3$, as well as in 23–24 UT, where the density reached $3 \times 10^{12}\text{el}/\text{m}^3$, after a descent behavior that had started from 21 UT.

Correlation coefficients are calculated between the irregularity indexes and the ionospheric parameters for the period of high variability of electrons. Between the irregularity indexes and $h'F$, the correlation is around 0.42, with *hmF2* about 0.62, and with *NmF2* close to 0.71, which indicates a moderate correlation between the values.

The same analysis can be applied with respect to the estimated indexes for station CEFT and the ionospheric parameters of the ionosonde Fortaleza for Days A and B. Regarding the correlations between the irregularity indexes with $h'F$, the values are about 0.49, whereas with *hmF2* they are 0.51 and with *NmF2* 0.74. For station BOAV and the ionosonde Boa Vista, as well as for station CEFT and the ionosonde Fortaleza, the obtained correlations are moderate, with the exception of correlations with the *NmF2* parameter which is classified as strong. One reason for moderate correlations is the differences between sampling intervals of irregularity indexes (1 h, 15 and 5 min) and the $h'F$, *hmF2*, and *NmF2* parameters (10 min).

Indexes for CEFT are computed to verify the estimate of the indexes of ionospheric irregularities for a period of low ionospheric irregularities for June 11, 2014 (Day C), which is near the winter solstice, and with D_{st} values oscillating close to 0 nT. The mask angle is 35°. On this day, all indexes are below the thresholds of low levels of irregularities of the ionosphere, supported by the low values of $h'F$, about 210 km, *hmF2* 270 km, and *NmF2* $1.4 \times 10^{12}\text{el}/\text{m}^3$. The correlation coefficients oscillate around 0.54 for $h'F$ and *hmF2* and are close to 0.91 for *NmF2*. These values indicate the correspondence between the classification of irregularities by indexes and by ionospheric parameters.

The analyses carried out for Days A, B, and C indicate that the estimates of the ionospheric irregularity indexes from GNSS data are consistent. However, it is worth noting that only two digital ionosonde values are used, since only these are available for the days under review.

The same days of high variation of electron density previously used and Day D (June 7, 2014) are considered for the assessment of the phase scintillation indexes σ_Φ, S_Φ, and σ_{CHAIN}. Indexes are estimated for six stations: INCO (22.3°S, 46.3°W), PALM (10.2°S, 48.3°W), POAL (30.1°S, 51.1°W), PRU1 (22.1°S, 51.4°W), SJCE (23.2°S, 45.9°W), and UFBA (13.0°S, 38.5°W). The Ion_Index uses the phase measurements contained in the station observation files, with sampling rate of 0.067 Hz, for the estimation. The graphics of σ_Φ index are also obtained through the Ionospheric Scintillation Monitoring Receiver (ISMR) Query Tool for these same stations and period of time. The ISMR Query Tool is a web tool that enables access to the σ_Φ values from CIGALA/CALIBRA network stations. These values are available from Septentrio PolaRxS-PRO receivers, through calculations and application of the Butterworth detrending method of the raw data, which are sampled in 50 Hz. In both programs, an elevation mask of 35° is considered. Thus, each selected station we have the σ_Φ index from the ISMR Query Tool, which is considered the "true value", and the σ_Φ index estimated by Ion_Index, as well as the S_Φ and σ_{CHAIN} indexes. The results are compared in order to assess the estimate of the indexes.

Figure 5 is an example showing the phase scintillation indexes estimated by Ion_Index, as well as the σ_Φ index of ISMR Query Tool (top row), of stations POAL, PRU1, and UFBA for Day B. The green line in the graphics indicates the boundary between weak and moderate ionospheric scintillation, while the red line indicates the boundary

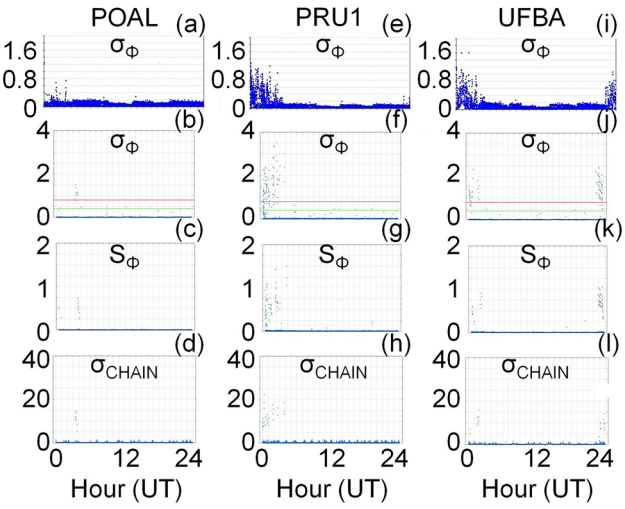

Fig. 5 Scintillation indexes of stations POAL, PRU1, and UFBA on Mar. 1, 2014. Panels **a**, **e**, and **i** are σ_Φ indexes from ISMR Query Tool, and the remaining panels are indexes from Ion_Index

between moderate and strong levels. Only values for the L1 carrier are shown.

In Fig. 5, considering only the values of the σ_Φ index from the specialized receivers (top row) and the values estimated by the algorithm (second row), it can be seen that the behavior of the values is similar. In the occurrence of ionospheric scintillation, the estimated values identify the event at the same instant and with the same duration as the known values, as well as in the non-occurrence of scintillation, where the estimated and known values remain below the threshold of low scintillation. Panels (a–d) show that in station POAL there is no scintillation of GNSS signals. For PRU1 there is scintillation during the first hours, as can be seen from the peaks of the indexes in the panels (e–h). The temporal and behavioral correspondence of the estimated and known σ_Φ values is more evident if analyzed alongside the graphics of UFBA in the panels (i–l). The behavior of estimated and known values is also similar for the period of low variability of electron density.

However, Fig. 5 also shows that during the non-occurrence of ionospheric scintillation the values of the estimated σ_Φ index are lower than those provided by the web tool, unlike the situation in which scintillation occurs, where values are higher than those considered true. This behavior of the estimated values is justified by the methodology used to accomplish the detrending of carrier phase measurements Φ_e, as well as by the data sampling rate. In the case of σ_Φ values from the ISMR Query Tool, the phase measurement sampling is 50 Hz, totaling 3000 measurements to determine the standard deviation, and the Butterworth detrending method is applied. The Ion_Index sampling is 0.067 Hz, providing only five measurements for the calculation, and detrending boils down in controlling the multipath through the application of an elevation mask of 35° and detecting the loss of cycles. This accounts for the low correlation obtained for the period of high electron variability between the true and the estimated σ_Φ index, which is on average 0.55 considering the six stations. Regarding the S_Φ and σ_{CHAIN} indexes, the correlations obtained are 0.38 and 0.25, respectively. However, the obtained correlations are high for Day D, having values around 0.76, 0.65, and 0.60 between σ_Φ true with σ_Φ estimated, S_Φ, and σ_{CHAIN}, respectively.

Thus, the possibility of identifying the occurrence of ionospheric scintillation and its duration. An estimate of its intensity could be analyzed from carrier phase measurements and evaluated positively since there is agreement between the values. The estimated index shows the same classification for all situations in which ionospheric scintillation is classified as strong by the known index. Concerning the S_Φ and σ_{CHAIN} indexes, it can be observed from Fig. 5 that their behaviors are analogous to the σ_Φ index, indicating the possibility of using these other indexes for analysis of the GNSS signals phase scintillations.

Analysis of the seasonal variation during the peak of solar cycle 24

Irregularity and scintillation indexes are estimated from February 15 to March 15 (Period A) and from June 15 to July 15 (Period B) for the years 2013, 2014, and 2015, which are a total of 180 days close to the equinox and solstice. All available stations of the Brazilian networks are used, with a 35° of elevation mask. Values of seven stations are presented for exemplification purposes: CUIB (15.6S, 56.1W), NAUS (3.0S, 60.1W), POAL, RECF (8.1S, 35.0W), SJRP (20.8S, 49.4W), SSA1 (13.0S, 38.5W), and TOPL (10.2S, 48.3W), contemplating the tropical and mid-latitudes regions. Figure 6 shows the results of the indexes for the day of maximum variability of electron density, which corresponds to Day B. It is worth noting that only the scintillation indexes for the L1 carrier are presented.

In general, Fig. 6 shows that the irregularities and scintillation indexes are higher for the period of maximum variability of electron density (close to the autumnal equinox) than the period of low variability (near the winter solstice).

During Period A, the irregularity indexes reached values which classify as moderate to strong, especially on March 1, 2014, where results are more accentuated, as can be seen in Fig. 6, panels (a–d). In relation to the ionospheric scintillations, it is verified that the phase scintillation

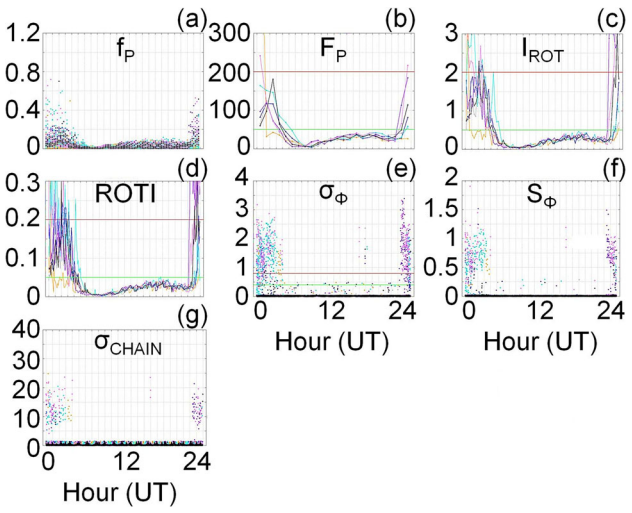

Fig. 6 Irregularity indexes of stations CUIB (*blue*), NAUS (*gray*), POAL (*yellow*), RECF (*purple*), SJRP (*cyan*), SSA1 (*pink*), and TOPL (*black*) on Mar. 1, 2014

indexes increase with the occurrence of strong and moderate irregularities.

Analyzing each station of Fig. 6, it can be seen that RECF, SJRP, and SSA1 have index values of irregularity and scintillation higher than CUIB, NAUS, and TOPL. This is due to the effects of and geographical behavior of the Equatorial Ionization Anomaly (EIA). The stations RECF, SJRP, and SSA1 are located near the anomaly's southern crest, while the other stations are close to the magnetic equator, where ionization is less intense. Concerning the station POAL, despite showing signs of irregularities and ionospheric scintillation during the first hours of the day, overall the values are lower than at other stations, due its location in the region of the mid-latitudes. In quantitative terms of F_P, none of the stations presents a value higher than 200, with the exception of POAL and SSA1. However, analyzing the other indexes, it appears that the irregularities are more intense, with some regions being classified as strong. The fact that the F_P index shows a value higher than 300 for the first hour at the station POAL in panel (b) is due to an extrapolated value of f_P during the instants 15 and 20 min. If the value was right, probably the phase scintillation indexes would indicate a strong scintillation for the period; however, this did not occur.

For Period B, all stations present irregularity indexes classified as low. But results of σ_Φ, S_Φ, and σ_{CHAIN} for the station NAUS, during 19–20 UT on June 7, 2014, indicate the occurrence of strong ionospheric scintillation, which may indicate that small-scale ionospheric irregularities and low intensity can also cause scintillations on GNSS signals.

Concerning the scintillation indexes proposed by Forte (2005) and Mushini et al. (2012), it is observed that, in the occurrence of ionospheric scintillations detected from σ_Φ values, the S_Φ and σ_{CHAIN} values also identify it at the same instant of occurrence and with the same duration. Therefore, they can also be used for analysis of ionospheric scintillations.

As an example for visualization of spatial and temporal behavior of ionospheric irregularities, we show maps of the F_P index for Days B and D, respectively, in Figs. 7 and 8. The presentation sequence of maps is from left to right, top to bottom. All available stations of the Brazilian ACSs are used for the generation of maps, with an elevation mask of 35°.

Figure 7 shows the spatial and temporal displacement of ionospheric irregularities along the magnetic equator over Brazil, from northeast to southwest, starting at 22 UT (19 local time) and ending at 5 UT (2 local time). The presence of irregularities is not observed in Fig. 8 because it is a period of low electron density. These two different situations of occurrence and non-occurrence of ionospheric irregularities for a period near the autumn equinox and

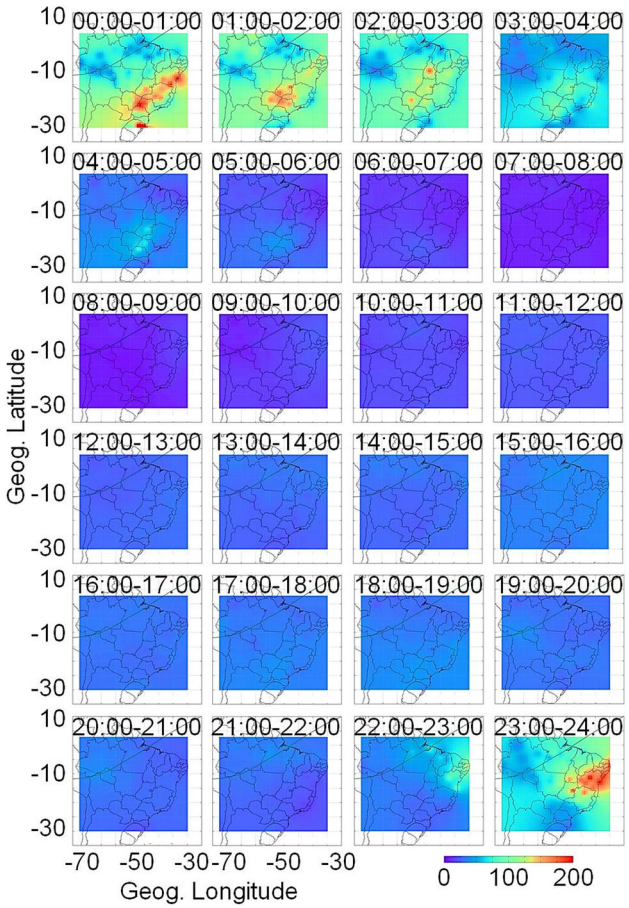

Fig. 7 F_P maps over Brazil on Mar. 1, 2014. Time interval of each map is 1 h. Time is in UT. The *color scale* of F_P index is between 0 (*blue*) and 200 (*red*)

close to the winter solstice is one way to characterize the seasonal variation.

One of the disadvantages regarding the use of the F_P index in monitoring is due to temporal resolution, 1 h, making a more accurate monitoring of irregularities impossible. Using the f_P, I_{ROT}, and *ROTI* indexes can achieve a better understanding of the evolution of irregularities due to the lower time interval to obtain the indexes. Maps of f_P and *ROTI* indexes for 22–24 UT of Day B are presented in Figs. 9 and 10, respectively. An elevation mask of 35° is also used.

Figure 9 shows that the f_P maps allow a better geographical understanding of ionospheric irregularities because the values are determined at the IPP positions. Depending on the angle of the elevation mask, the occurrence of ionospheric irregularities south and north of the magnetic equator can be identified, as well as on the Brazilian oceanic coast, a region little explored in ionospheric terms. Analyzing the period 23:45–24 UT, it is noted that the irregularities affected an area south of the magnetic equator of approximately four million square

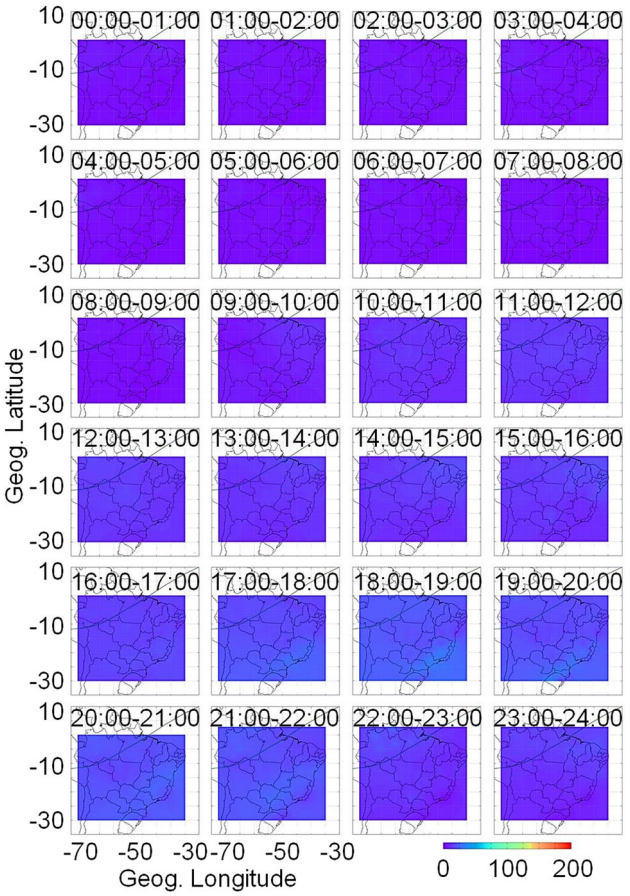

Fig. 8 F_P maps over Brazil on June 7, 2014. Time interval of each map is 1 h. Time is in UT. The *color scale* of F_P index is between 0 (*blue*) and 200 (*red*)

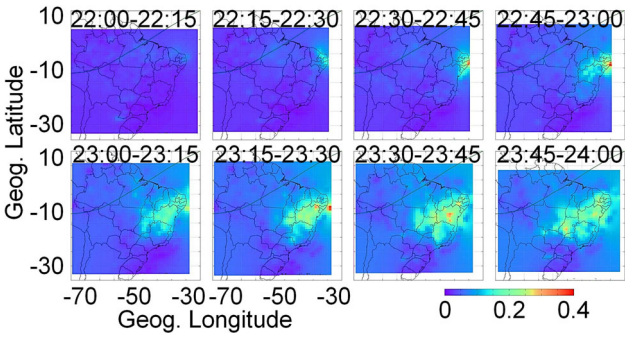

Fig. 9 f_P maps over Brazil for 22–24 UT on Mar. 1, 2014. Time interval of each map is 15 min. The *color scale* of f_P index is between 0 (*blue*) and 0.4 (*red*)

kilometers, with a maximum longitudinal length of 2350 km and maximum latitudinal length of 1800 km.

The *ROTI* maps from Fig. 10 enable a better temporal understanding of the irregularities due to temporal resolution which is only five minutes.

Regarding the phase ionospheric scintillations, σ_Φ maps are provided for the period in which the irregularity levels

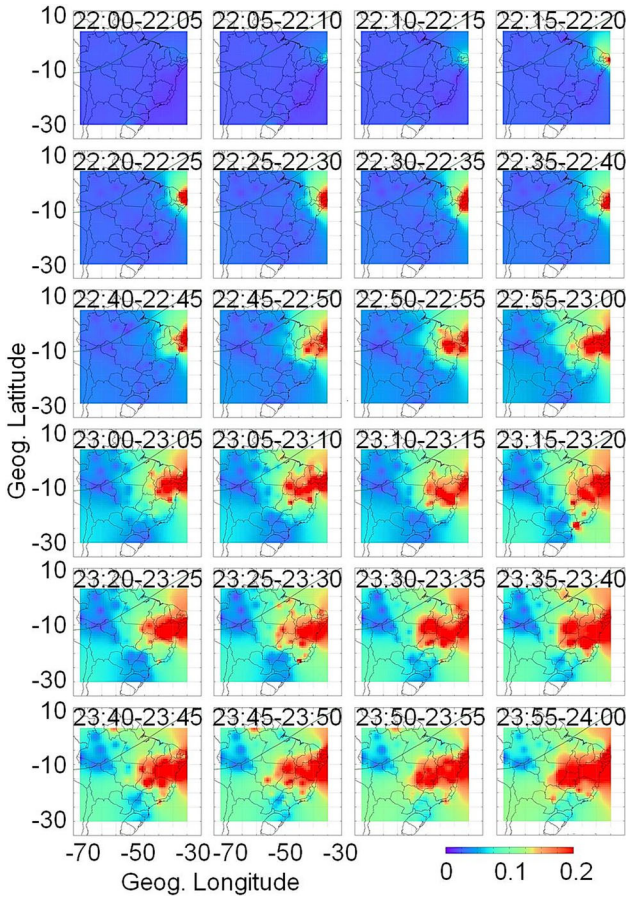

Fig. 10 *ROTI* maps over Brazil for 22–24 UT on Mar. 1, 2014. Time interval of each map is 5 min. The *color scale* of *ROTI* index is between 0 (*blue*) and 0.2 (*red*)

are high, i.e., 22–24 UT Day B. All available stations are used. Figure 11 shows maps for the L1 carrier, using an elevation mask of 35°.

Comparing Fig. 11 with 9 and 10, a correspondence can be seen between the occurrences of irregularities with the ionospheric scintillation events. It is possible to identify the locations where the scintillations are stronger inland and at the coastal region. Maps of S_Φ and σ_{CHAIN} indexes are not shown because of the similarity with the σ_Φ maps.

Monitoring of irregularities and scintillations from indexes and maps proved a valid tool, which can in turn be used to develop models to minimize the effects of the ionosphere, especially on positioning techniques.

Monitoring of ionospheric irregularities and ionospheric scintillations in real-time

The real-time monitoring is performed using the Ion_Index_RT mode for the period of December 20–26, 2014, with D_{st} values ranging from 0 to −50 nT. These days are

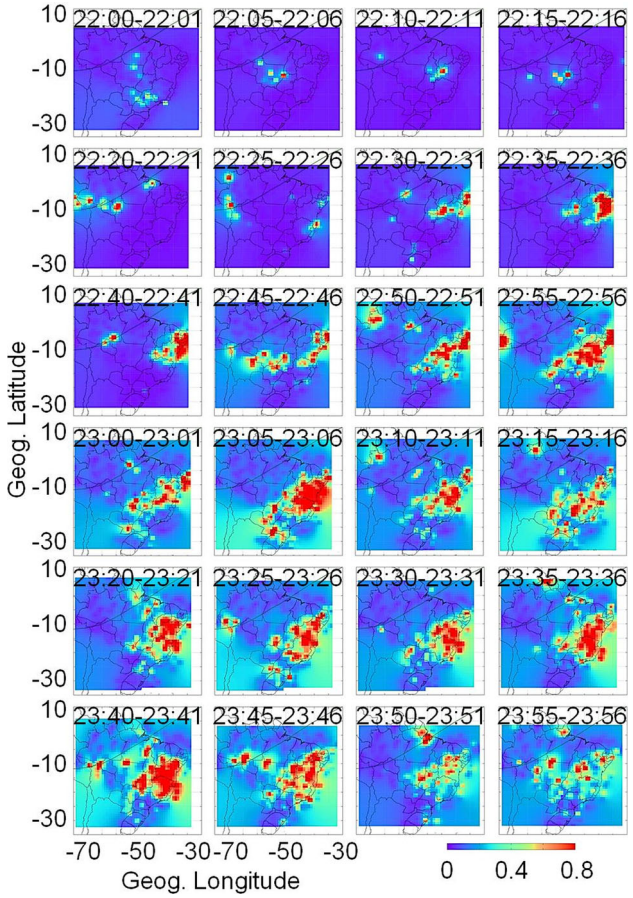

Fig. 11 σ_Φ maps over Brazil for 22–24 UT on Mar. 1, 2014. Time interval of each map is 1 min. The *color scale* of σ_Φ index is between 0 (*blue*) and 0.8 (*red*)

Table 1 RBMC-IP stations selected for the monitoring of ionospheric irregularities and ionospheric scintillations in real-time

Station	Latitude	Longitude	Station	Latitude	Longitude
BOAV	2.8N	60.7W	NAUS	3.0S	60.1W
BOMJ	13.3S	43.3W	POAL	30.1S	51.1W
BRAZ	15.9S	47.9W	POVE	8.7S	63.9W
CRAT	7.2S	39.4W	PRCV	25.0S	53.5W
CRUZ	7.6S	72.7W	RECF	8.1S	35.0W
GVA1	18.9S	42.0W	RNNA	5.8S	35.2W
ILHA	20.4S	51.3W	ROCD	13.1S	60.5W
MABA	5.4S	49.1W	SALU	2.6S	44.2W
MAPA	0.1N	51.1W	SSA1	13.0S	38.5W
MSCO	19.0S	57.6W	TOGU	11.7S	49.0W
MTCO	10.8S	55.5W	UBA1	23.5S	45.1W

characterized by high electron variability rates due to the summer solstice in the southern hemisphere. Table 1 presents the names and coordinates of the twenty-two stations used.

The following order of monitoring is established: f_P (20), F_P (21), I_{ROT} (22), *ROTI* (23), σ_Φ (24), S_Φ (25), and σ_{CHAIN} (26). Instants of real-time visualization in which strong irregularities and scintillations occurred are shown in the left column of Fig. 12. In order to examine the reliability of the real-time mode, the values and maps in the post-processed mode are estimated for each of the indexes and their respective days, considering the same stations in Table 1 and using 35° of elevation mask (right column).

In general, from viewing Fig. 12 it can be concluded that the spatial and temporal correspondences of ionospheric irregularities and scintillation of GNSS signals from post-processed and real-time modes achieved a significant level of agreement. The monitoring of the irregularities presents better results from f_P, F_P, and *ROTI* indexes, as can be seen in the panels (a–d) and (g) and (h). In relation to the I_{ROT} index of the panels (e) and (f) it can be observed that the strong ionospheric irregularities are determined differently in the real-time and post-processed modes. Several reasons that can justify this fact include: Outliers or cycle slips were not correctly detected in real-time, a problem inherent in GNSS stations, or the number of stations for real-time processing is lower than for the post-processed mode. In terms of ionospheric scintillation monitoring, first in relation to the σ_Φ index, no area of scintillation occurrence is detected for December 24 in panels (i) and (j). Yet, for December 25 and 26, the occurrence of ionospheric scintillations is mapped similarly by S_Φ and σ_{CHAIN} indexes in the two modes, as shown in the panels (k–n).

Practical application of the indexes in the analysis of Precise Point Positioning results

A practical application of the indexes and maps of irregularities and scintillation is the analysis of GNSS positioning. Thus, two experiments have been performed: (a) static Precise Point Positioning (PPP) of the station PRU1 for March 1, 2014, and (b) kinematic PPP of station RNNA for December 23, 2014. The online software IBGE-PPP (http://www.ppp.ibge.gov.br/ppp.htm) is used for the processing of the data.

Figure 13 presents the static PPP results, where panel (a) shows the horizontal discrepancy Δ_{horiz} (blue line) in the local geodetic system and its standard deviation σ_{horiz} with 95% confidence level (red line). Panel (b) shows the vertical discrepancy Δ_{vert} (blue line) and the standard deviation σ_{vert} (red line). Panels (c–e) show the irregularity indexes, and panel (f) shows the σ_Φ index. A mask of 35° is applied in all graphics.

In Fig. 13, the times when the horizontal discrepancy is more than 20 cm and the vertical is less than −60 cm, and

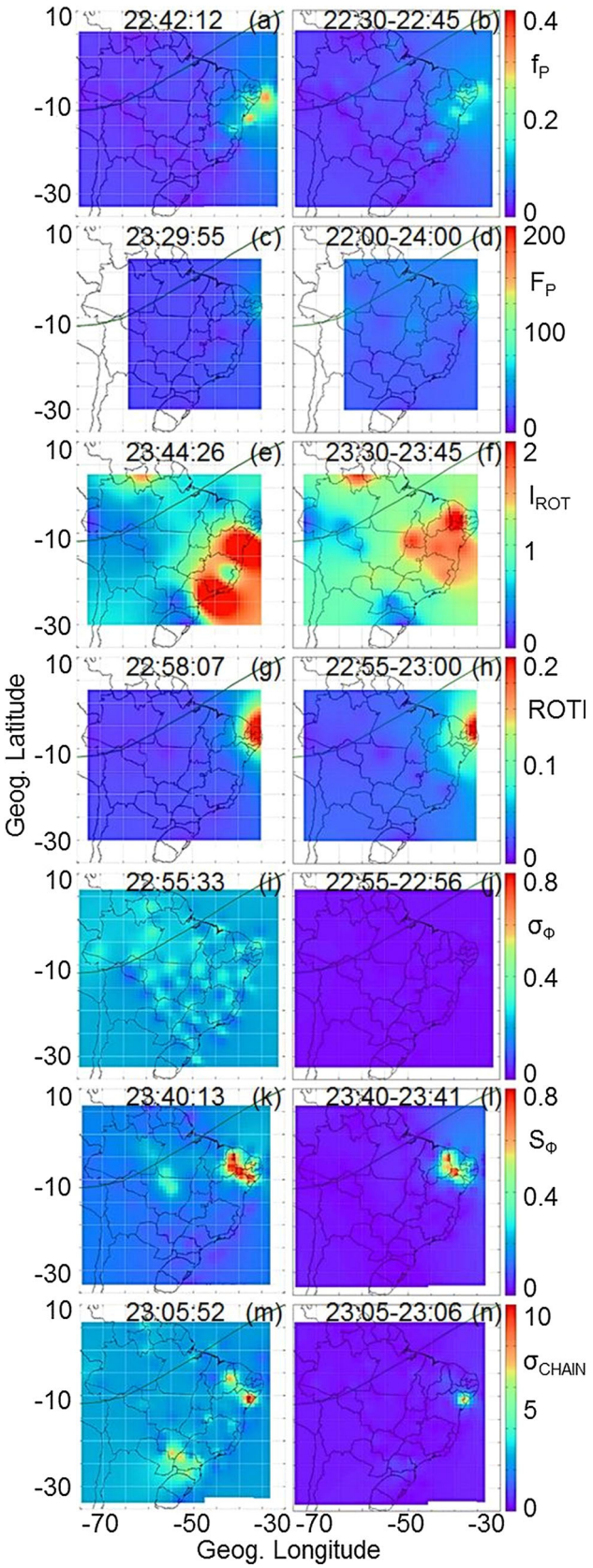

◀**Fig. 12** Maps of ionospheric irregularities and ionospheric scintillations over Brazil in real-time (*left column*) and post-processed (*right column*) for Dec. 20 (*top row*) to 26 (*bottom row*), 2014. Hour is in UT

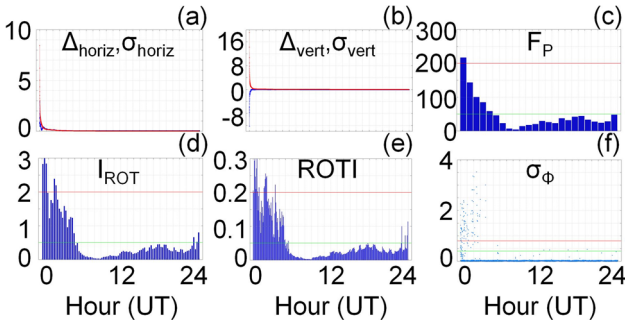

Fig. 13 Horizontal and vertical discrepancies and their standard deviations from static PPP, panels **a** and **b**, and irregularity and scintillation indexes of station PRU1, panels (**c–f**), on Mar. 1, 2014. In panels **a** and **b**, the unit is meters and the discrepancies are in *blue* and the standard deviations in *red*

the instants when the respective standard deviations deteriorate, coincide exactly with the peak of ionospheric irregularities, panels (c–e), and with the occurrence of strong ionospheric scintillations, panel (f). We conclude that the positioning degradation is correlated to the ionospheric activity in the region. For the remaining hours of the day, the horizontal and vertical discrepancies oscillate around 3.7 and 4.1 cm, respectively, according to the level of ionospheric irregularities, which is classified as low for the rest of the day. Figure 7 shows the irregularities over the period in which discrepancies and accuracies deteriorate.

Figure 14 shows the horizontal and vertical discrepancies and the standard deviations of RNNA kinematic PPP, simulating a real-time processing, as well as the F_P, I_{ROT}, *ROTI*, and σ_Φ indexes.

In Fig. 14, it can again be noted that the degradation of discrepancies and accuracies correlates with the occurrence of strong ionospheric irregularities. As it turns out, the variability of the horizontal and vertical discrepancies during the period 00–04 UT, reaching maximums of 2 m in Δ_{horiz} and 8 m in Δ_{vert} at 02:30 UT, and the variability of the intensity of ionospheric irregularities show a moderate peak also at 02:30 UT.

The panel (g) of Fig. 12 shows the exact moment at 23 UT when there is an increase in irregularities, also shown by the irregularity indexes of Fig. 14, corroborating with the instant of elevation of the standard deviation of horizontal (maximum of 1.41 m) and vertical (maximum of

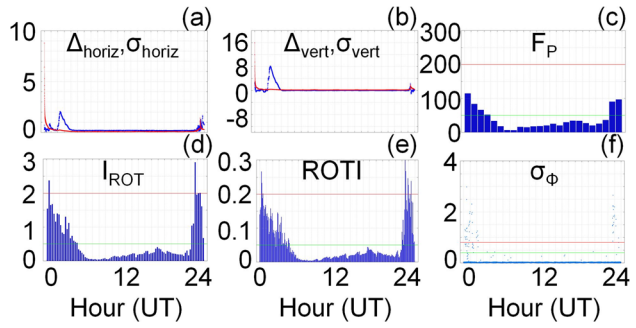

Fig. 14 Horizontal and vertical discrepancies and their standard deviations from kinematic PPP, panels **a** and **b**, and irregularity and scintillation indexes of station RNNA, panels (**c**–**f**), on Dec. 23, 2014. In panels **a** and **b**, the unit is meters. The discrepancies are in *blue* and the standard deviations in *red*

1.91 m) components of the panels (a) and (b) of Fig. 14. The real-time monitoring of the displacement of ionospheric irregularities allows decision-making whether or not to perform positioning in the region under ionospheric effects.

Conclusions

The transformation of the GNSS-SP and RBMC network stations, widely used for positioning purposes, into ionospheric monitoring systems using the presented method provides a wider set of information about the ionosphere in Brazil. These stations serve the development and improvement of mitigation models, as well an increase in spatial resolution, since the number of dedicated ionospheric monitoring in Brazil is small. This densification allows a better understanding of the dynamics of the main ionospheric effects in Brazil: ionospheric irregularities and scintillation of GNSS signals.

From the experiments, it can be seen that ionospheric irregularities start at approximately 22 UT (19 local time) in the Brazilian northeast, moving over the territory in a northeast–southwest direction along the magnetic equator, and ionospheric scintillations occur in regions where the irregularity levels are higher.

Regarding the irregularity indexes investigated, it is concluded that the *ROTI* should be used for the study of temporal variation of ionospheric irregularities, while the spatial study is borne by the f_P. The F_P index is used for general purposes. Concerning phase scintillations, due to a low data sampling rate, the implemented σ_Φ index enables identification of the occurrence and duration of ionospheric scintillation and an estimate of its intensity.

The study and monitoring of the ionosphere using specialized equipment such as ionosondes, imagers, radars, and geodetic receivers like Septentrio PolaRxS-PRO are the most appropriate forms that currently exist. However, the high cost makes it impossible to establish a dense network over the 8.5 million square kilometers of national territory. Therefore, the indexes calculated with GNSS active network data serve as an alternative for the densification of information about irregularities and scintillation of the ionosphere, because it uses infrastructure already deployed by RBMC, GNSS-SP, and CIGALA/CALIBRA.

The experiments validate the proposed method for the estimation of the indexes of ionospheric irregularities and phase scintillations, because the results are compared with data from external sources and proved compatible with moderate to high correlations in the situations of high and low variability of electrons.

Experiments using indexes of irregularities and scintillation are carried out in order to verify the effects of seasonal variation during the peak of solar cycle 24. Maps are produced, allowing the identification, limitation, and displacement of irregularities.

Real-time monitoring is carried out for the period of the summer solstice, where the results obtained are consistent with those from the post-processed mode.

Indexes and maps of irregularities and scintillation can be applied to analyze the results of GNSS positioning, such as in the static and kinematic PPP. The results make clear that the degradation of horizontal and vertical coordinate estimates, along with the standard deviations, are correlated to the intensity of ionospheric irregularities, and consequently to the ionospheric scintillations.

Real-time ionospheric information can be used in important practical applications, such as precision agriculture, approach and landing of aircraft, monitoring of oil rigs and structures, RTK, because the monitoring of the displacement of ionospheric irregularities allows decision-making to accept or reject the results of positioning.

As a recommendation, IBGE has the supply of RINEX files of RBMC stations with data sampling rate higher or equal to 1 Hz, which would allow a more accurate estimation of phase scintillations.

Acknowledgements Our thanks go to the funding agencies CAPES (Coordination for the Improvement of Higher Education Personnel), FAPESP (Sao Paulo Research Foundation—process 2013/19147-1), and CNPq (National Council for Scientific and Technological Development—processes 479965/2013-7 and 309924/2013-8) for financial support, to the IBGE, the CIGALA/CALIBRA projects, the Spatial Geodesy Laboratory for the supply of GNSS data, and to INPE for the digital ionosonde data.

References

Blewitt G (1990) An automatic editing algorithm for GPS data. Geophys Res Lett 17(3):199–202

Bremer J, LjR C, Mielich J, Stamper R (2006) Derivation and test of ionospheric activity indices from real-time ionosonde observations in the European region. J Atmos Sol Terr Phys 68(18):2075–2090

Campbell WH (1996) Geomagnetic storms, the Dst ring-current myth and lognormal distributions. J Atmos Terr Phys 58(10):1171–1187. doi:10.1016/0021-9169(95)00103-4

Chu FD, Lee CC, Chen WS, Liu JY (2008) A study of long-term climatology of ionospheric irregularities by using GPS phase fluctuations at the Brazilian longitudes. J Adv Space Res 41(4):645–649

Conker RS, El-Arini MB, Hegarty CJ, Hsiao T (2003) Modeling the effects of ionospheric scintillation on GPS/satellite-based augmentation system availability. Radio Sci 38(1):1–23

Davies K (1990) Ionospheric radio. Peter Peregrinus Ltd, London

Forte B (2005) Optimum detrending of raw GPS data for scintillation measurements at auroral latitudes. J Atmos Sol Terr Phys 67(12):1100–1109. doi:10.1016/j.jastp.2005.01.011

Gulyaeva TL, Stanislawska I (2008) Derivation of a planetary ionospheric storm index. Ann Geophys 26(9):2645–2648 **Copernicus GmbH**

Gulyaeva TL, Arikan F, Hernandez-Pajares M, Stanislawska I (2013) GIM-TEC adaptive ionospheric weather assessment and forecast system. J Atmos Sol Terr Phys 102:329–340. doi:10.1016/j.jastp.2013.06.011

Hegarty C, El-Arini MB, Kim T, Ericson S (2001) Scintillation modeling for GPS-wide area augmentation system receivers. Radio Sci 36(5):1221–1231

Jakowski N, Hocke K, Schlüter S, Heise S (1999) Space weather effects detected by GPS based TEC monitoring. In: Proceedings workshop on space weather, WPP-155, ESTEC, Noordwijk, 241–244

Jakowski N, Borries C, Wilken V (2012) Introducing a new disturbance ionosphere index. Radio Sci. doi:10.1029/2011RS004939

Klobuchar J (1996) Ionospheric effects on GPS. In: Parkinson BW, Spilker JJ, Axelrad P, Enge P (eds) Global positioning system: theory and applications, I edn. Am Inst. of Aeronaut, and Astronaut., New York, pp 485–515

Matsuoka MT, Camargo PO (2004) Determination of TEC using GPS data from dual frequency receivers for the production of ionosphere maps to Brazil. Revista Brasileira de Cartografia 1(56):14–27

Mendillo M, Lin B, Aarons J (2000) The application of GPS observations to equatorial aeronomy. Radio Sci 35(3):885–904

Mielich J, Bremer J (2010) A modified index for the description of the ionospheric short and long-term activity. Ann Geophys 28(12):2227–2237. doi:10.5194/angeo-28-2227-2010 **Copernicus GmbH**

Mushini SC, Jayachandran PT, Langley RB, MacDougall JW, Pokhotelov D (2012) Improved amplitude-and phase-scintillation indices derived from wavelet detrended high-latitude GPS data. GPS Solut 16(3):363–373

Oladipo OA, Schüler T (2013) Equatorial ionospheric irregularities using GPS TEC derived index. J Atmos Sol Terr Phys 92:78–82

Pereira VAS, Camargo PO (2013) Estimation and analysis of the ionosphere irregularities indices using GPS data from active networks. Bol Ciênc Geod 19(3):374–390

Pereira VAS, Camargo PO (2014) Padrões para classificação dos índices de irregularidades da ionosfera: I_{ROT} e ROTI. In: Anais do V Simpósio Brasileiro de Ciências Geodésicas e Tecnologias da Geoinformação da Universidade Federal de Pernambuco, pp 547–555

Pereira VAS, Camargo PO (2016) Scientific program for monitoring in real time or post-processed of ionospheric irregularities and scintillation of GNSS signals. Bol Ciênc Geod 22(2):282–302

Pi X, Mannucci AJ, Lindqwister UJ, Ho CM (1997) Monitoring of global ionospheric irregularities using the worldwide GPS network. Geophys Res Lett 24(18):2283–2286

Shan SJ, Liu JY, Kuo FS, Liu CC, Tsai HF (2002) GPS phase fluctuations observed along the American sector during low irregularity activity months of 1997–2000. Earth Planets Space 54(2):141–152

Van Dierendonck AJ, Klobuchar J, Hua Q (1993) Ionospheric scintillation monitoring using commercial single frequency C/A code receivers. In: Proceedings of the ION GPS 93, Institute of navigation, Salt Lake City, USA, 1333–1342

Wanninger L (1993) Ionospheric monitoring using IGS data. In: Beutler G, Brockmann E (Eds) Proceedings of the 1993 IGS workshop, Astronomical Institute, University, of Berne, 351–360

Vinícius Amadeu Stuani Pereira received his BE degree in Cartographic Engineering in 2012 and M.Sc. degree in Cartographic Sciences in 2015 from Universidade Estadual Paulista (UNESP) at Presidente Prudente, SP, Brazil. He is a Ph.D. candidate at UNESP, and the focus of his current research lies in developing a Brazilian Ionospheric Threat Model for GBAS in the GNSS context.

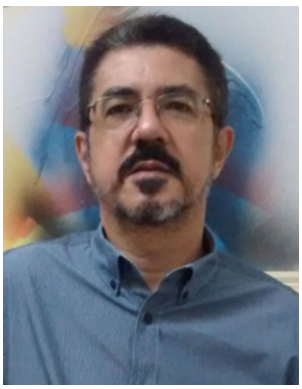

Paulo de Oliveira Camargo received his BE degree in Cartographic Engineering in 1985 from Universidade Estadual Paulista (UNESP), his M.Sc. degree in 1992 and Ph.D. degree in 1999 in Geodetic Sciences from the Universidade Federal do Paraná (UFPR), Brazil. He is professor of the graduate and postgraduate program at UNESP focusing on the following topics: GNSS, ionosphere, quality control, and least-squares adjustment.